Original Article

PORTO BIOMEDICAL JOURNAL
WHERE SCIENCE MEETS KNOWLEDGE

OPEN

Prediction of MMP-9 inhibitory activity of N-hydroxy-α-phenylsulfonylacetamide derivatives by pharmacophore based modeling and 3-D QSAR studies

Dharmender Rathee, MS[a], Viney Lather, PhD[b], Harish Dureja, PhD[a,*]

Abstract

Matrix metalloproteinase-9 (MMP-9), also known as gelatinase B, is a MMP that is strongly associated with multiple cellular processes including proliferation, angiogenesis, and metastasis. Various studies have shown that N-hydroxy-α-phenylsulfonylacetamide (HPSAs) derivatives are promising and selective for the MMP-9 inhibition. In the present study, we have selected and reported 80 HPSAs derivatives as inhibitors of MMP-9 and performed structure-based 3-dimensional quantitative structure–activity relationship (3D-QSAR) studies to elucidate the important structural elements responsible for binding affinity. Developed pharmacophore models; QSAR model I contains 2 hydrogen-bond acceptors (A), 2 hydrogen-bond donors (D), and 1 aromatic ring (R) and QSAR model II contains 3 hydrogen-bond acceptors (A), 1 positive ionic (P), and 1 aromatic ring (R). The statistical results of QSAR models (I and II) such as good correlation coefficient (0.61 for I and 0.63 for II), good predictive power (0.84 and 0.77 for I and II, respectively) with low standard deviation (SD\0.3 for both) strongly suggest that the developed models are virtuous for the future prediction of MMP-9 inhibitory activity of HPSAs derivatives. The geometry and features of pharmacophore were expected to be useful for further design and development of selective MMP-9 inhibitors.

Keywords: 3D-QSAR, MMP inhibitors, MMP-9 (92 kDa), N-hydroxy-α-phenylsulfonylacetamide derivatives, pharmacophore based modeling

Introduction

The matrix metalloproteinase (MMP) family consists of at least 23 structurally related zinc-dependent endopeptidases enzymes, sharing several specific functional and structural components. These enzymes selectively break down many components of the extracellular matrix (ECM) releasing growth factors and cytokines, and play a key role in many constitutive processes, including embryogenesis, normal tissue remodeling, and angiogenesis. Over the years, several studies have indicated that enzymes such as MMPs are the primary mediators of the microenvironment changes seen during cancer progression.[1] They have a significant role in pathological conditions, such as atheroma, arthritis, cancer, and tissue ulceration, as well.[1–5] Furthermore, due to their proteolytic activity, they are very important in tumor invasion and metastasis, being overexpressed in several types of human cancer. Also, they are accountable for regulating pathways of cell growth, survival, inflammation, and angiogenesis, which are crucial factors for tumor progression.[6] Concerning the subtypes of MMP involved in cancer progression, MMP-2 and MMP-9 have been associated with tumor aggressiveness, metastatic potential, and poor prognosis in malignant neoplasms.[2,7] They are overexpressed in breast, brain, ovarian, pancreas, colorectal, bladder, prostate, lung cancers, and melanoma.[8] MMP-9, however, is also responsible for releasing several extracellular matrix factors, which promote proliferation and migration of endothelial cells involved in angiogenesis and tumor growth.[9] In this regard, the inhibition of MMP-2 and/or MMP-9 activity, as potential treatment for tumor progression, would be highly desirable. Amongst all, MMP-9 is particularly involved in inflammatory processes, bone remodeling, and wound healing. It is also implicated in pathological processes such as rheumatoid arthritis, atherosclerosis, tumor growth, and metastasis.[10–12] Difference in production levels of regulatory mechanisms of MMP-9 subsequently results in restricted, extensive, or improperly timed degradation of extracellular matrices.[13] The role of MMP-9 in many pathological diseases has laid a foundation for the identification of selective inhibitors. The structure of the MMPs includes a signal peptide, a propeptide, a catalytic domain with a highly conserved zinc-binding site, and a haemopexin-like domain, which is linked by a hinge region.[14] The structure of the catalytic domain of human MMP-9 (without the fibronectin repeats) consists of 5-stranded-sheet and 3-helices, which is similar to other MMPs. The catalytic center is composed

Sponsorships or competing interests that may be relevant to content are disclosed at the end of this article.

[a] Department of Pharmaceutical Sciences, Maharshi Dayanand University, Rohtak, [b] Department of Pharmaceutical Chemistry, JCDM College of Pharmacy, Sirsa, Haryana, India.

[*] Corresponding author. Department of Pharmaceutical Sciences, Maharshi Dayanand University, Rohtak-124001, India.
E-mail address: harishdureja@gmail.com (Harish Dureja).

Porto Biomed. J. (2018) 3:1(e6)

Received: 23 April 2018 / Accepted: 4 May 2018

http://dx.doi.org/10.1016/j.pbj.0000000000000006

of the active-site zinc ion, which is coordinated by 3 histidine residues (401, 405, and 411) and an essential water molecule.[15] MMP-9 is illustrious among the other MMPs by the incidence of 3 head to tail cysteine rich repeats which resemble fibronectin type II repeats. This insert is mandatory for their interaction with substrates like gelatin, laminin, and collagen.[16]

A wide range of medicinal chemistry approaches can be applied for designing new drug candidates, identifying potential hits, and accelerating the optimization of potential leads. Quantitative structure–activity relationship (QSAR) formalisms, for instance, are among the promising approaches in computer-assisted drug design (CADD) employed in the drug discovery process. Nowadays, structure-based drug design, molecular docking, and virtual high-throughput screening are widely used tools in the drug discovery. However, pharmacophore based drug design has proved to be a more efficient technique for the identification of potential new drug-like candidates, as this method provides the information about key structural features (in the form of an active pharmacophore) which are essential for biological activity. In modern computational biology, pharmacophores based approach is used to delineate the essential features of ≥1 molecules with the same biological activity. The pharmacophore based modeling of ligands is a well-established approach to quantitatively discover common chemical features among a considerable number of structures. Pharmacophore mapping can be used in designing the inhibitors in several ways, including justification of activity trends in molecules, searching of databases to find new chemical entities, and to identify important features for activity.[17]

In 2003, Aranapakam et al[18] reported N-hydroxy-α-phenyl-sulfonylacetamide derivatives (HPSAs) derivatives as the inhibitors of MMPs. These novel HPSAs derivatives were potent inhibitors of MMP-9, MMP-13, and moderate inhibitors of MMP-1. The selective inhibition of these compounds against gelatinases thus motivated to select these inhibitors to reveal the selectivity profile against MMP-9 and this can give clear picture on designing of molecules selectively towards MMP-9. Several studies of the relationships between MMP inhibitors and the structural features have been published.[19–23] Previous reported studies discussed various linear and non-linear QSAR[24,25] approaches against MMP-1, MMP-9, MMP-13, however, 3D-QSAR approach was not discussed. It was reported that the inhibitors of MMP-9 were potentially valuable for arresting tumor metastasis and also the inhibitors of MMP-13 could protect the cartilage degradation associated with osteoarthritis.[25] In this study, we have focused to design 3D-QSAR models against MMP-9 and to the best of our knowledge, no 3D-QSAR investigations for such kind of compounds have been reported till date. In the present study, a pharmacophore based drug design approach was used to identify the common set of features amongst a group of MMP-9 inhibitors resulting in development of a common pharmacophore model helping in the prediction of binding interactions with the MMP-9 enzyme. Furthermore, to uncover the important structural features responsible for the higher activity against MMP-9, we have performed 3D-QSAR studies on HPSAs.

Materials and methods

Software and hardware

The pharmacophore modeling and 3D-QSAR studies were carried out using PHASE version 3.0 as implemented in the Maestro 8.5 modeling package from Schrodinger, Molecular Modelling Interface Inc., LLC, NY installed on a Pentium IV 3.06 GHz, Core 2 Duo Quad PC with Windows 7 operating system.[26]

Dataset for analysis (biological data set)

The experimental dataset comprising of a series of 80 HPSAs derivatives was taken from the literature.[18,25] These compounds were discovered by Aranapakam et al[18] as MMP inhibitors and were used for the present study. In this study, two separate models were developed against MMP-9, that is, QSAR model I was developed for compounds 1 to 33 and QSAR model II was developed for compounds 34 to 80. In total 27 molecules were selected for QSAR model I, whereas 47 molecules were selected for QSAR model II. The in vitro biological activity data were reported as half maximal inhibitory concentration (IC_{50}). The IC_{50} values were converted to pIC_{50} using the formula ($pIC_{50} = -\log IC_{50}$). The dataset consisted of diverse range of molecules with highly active, inactive, and moderately active molecules. Figure 1 represents the common structure of the HPSAs derivatives employed and Tables 1 and 2 represent the substituents and the pIC_{50} values for all the compounds involved in this study. Out of 27 molecules used in the development of QSAR model I, 20 molecules were randomly chosen as training set and 7 molecules were selected

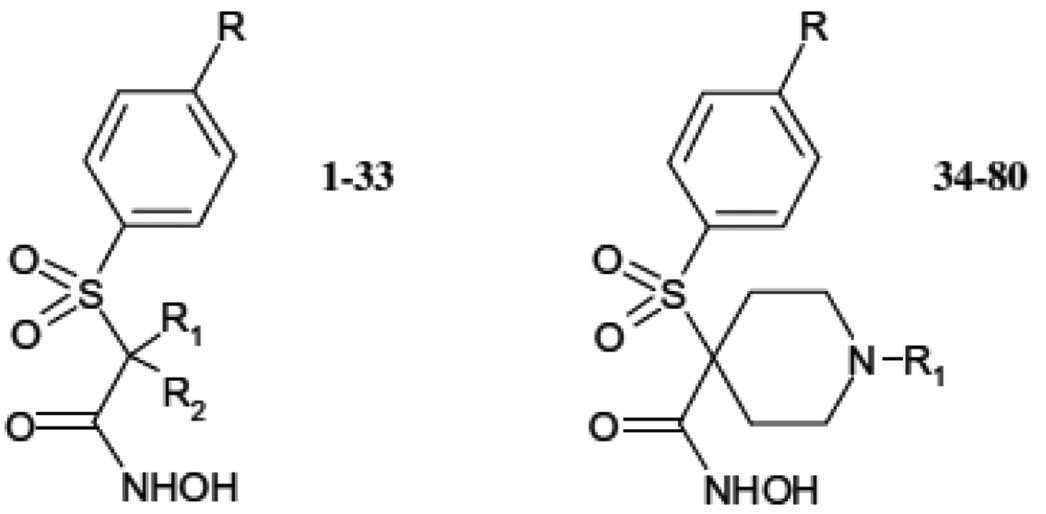

Figure 1. Structure of N-hydroxy-α-phenylsulfonylacetamide moiety.

Table 1

Chemical structures of HPSAs derivatives (compounds 1–33) employed for 3D-QSAR study along with predicted and actual pIC_{50} values against MMP-9 QSAR model I.

Compound (ligand name)	R	R1	R2	Actual pIC_{50}	Predicted pIC_{50}	Residual	Pharm set	Fitness
1*	OMe	Bn	H	3.97	3.86	−0.11	Moderate	2.72
2	OMe	Bn	Me	4.96	4.01	−0.95	Active	2.52
3	OMe	2-Naphthylmethyl	H	3.71	3.4	−0.31	Moderate	2.33
5*	OMe	4-Biphenylmethyl	Me	4.64	4.6	−0.04	Active	2.48
6	OMe	Isoprenyl	Me	4.96	4.01	−0.95	Active	2.57
9*	OMe	3-Phenylallyl	Me	4.8	4.32	−0.48	Active	2.59
10*	OMe	n-Pr	n-Pr	3.35	2.87	−0.48	Inactive	2.65
11	OMe	Iso Pr	H	0	2.69	2.69	Inactive	2.52
14*	OMe	n-dodecyl	H	2.53	2.4	−0.13	Inactive	1.77
15	OMe	Propargyl	Propargyl	3.85	3.39	−0.46	Moderate	1.96
16*	OMe	3-Picolyl	Me	4.42	4.08	−0.34	Active	3
17	OMe	3-Picolyl	Isoprenyl	5.05	3.95	−1.01	Moderate	2.38
18	OMe	3- Picolyl	IsoBu	4.2	3.62	−0.58	Moderate	2.27
19	OMe	3-Picolyl	IsoPentyl	3.92	3.14	−0.78	Inactive	2.21
20	OMe	3-Picolyl	n-Bu	0	1.71	1.71	Inactive	2.54
21	OMe	3-Picolyl	n-Octyl	3.76	3.27	−0.49	Inactive	2.41
22	OMe	3-Picolyl	Propargyl	4.08	3.51	−0.57	Active	2.25
23	OMe	4-[2-(1-Piperidinyl)ethoxy]benzyl	Me	5.05	4.97	−0.08	Active	2.51
24	OMe	4-[2-(1-Azepanyl)ethoxy]benzyl	Me	4.72	5.29	0.57	Active	2.71
25	OMe	4-[2-(Diisopropylamino)ethoxy]benzyl	Me	4.82	5.75	0.93	Active	1.77
26	OMe	4-[2-(Diethylamino)ethoxy]benzyl	Me	4.89	5.43	0.54	Active	2.75
27	OMe	4-{3-[4-(3Cl-phenyl)-1-piperazinyl]propoxy}benzyl	Me	5.15	6.1	0.95	Active	2.37
28	OMe	4-[2-(4-Morpholinyl)ethoxy]benzyl	Me	4.68	3.98	−0.07	Moderate	2.19
29*	OEt	4-[2-(Diethylamino)ethoxy]benzyl	Me	4.96	4.62	−0.34	Active	2.55
30	O-n-Bu	4-[2-(1-Piperidinyl)ethoxy]benzyl	Me	5.52	5.04	−0.48	Active	2.31
31	2-Furyl	4-[2-(Diethylamino)ethoxy]benzyl	Me	5.4	5.83	0.43	Active	2.48
33	Me	Isoprenyl	Isoprenyl	4.29	3.93	−0.36	Moderate	2.46

MMP-9 = matrix metalloproteinase-9; QSAR = quantitative structure–activity relationship.
* Test compounds.

as a part of test set, whereas out of 47 molecules used for the QSAR model II development, 37 molecules were randomly chosen as training set, and 10 were selected as a part of test set.

Phase methodology

"PHASE is a highly flexible program for pharmacophore perception, structural alignment, activity prediction and it provides support for lead discovery, SAR development, lead optimization, and lead expansion."[27] The step wise methodology used in the current study for the generation of pharmacophore models followed by development of 3D-QSAR models has already been discussed in previous publication by Lather et al.[28]

Ligand preparation. The LigPrep software (MMFF force field) implemented within PHASE was used for the 3-D conversion and minimization. All the structures were ionized at neutral pH 7. Conformers for each ligand were generated using ConfGen by applying OPLS-2005 force field method[29,30] with implicit GB/SA distance-dependent dielectric solvent model at cutoff root mean square deviation (RMSD) of 1 (MacroModel 9.6 2010) with 1000 iterations using water as solvent.

Pharmacophore model development. In order to create sites for all the ligands, a pharmacophore model generation uses a defined set of pharmacophoric features. In order to facilitate non-covalent binding between the ligand and its target receptor, each ligand structure coincides with various chemical features. In 3-D space, it is presented by a set of points. "PHASE module provides an in built set of 6 pharmacophore features, that is, hydrophobic group (H), hydrogen bond donor (D), hydrogen bond acceptor (A), aromatic ring (R), positively ionizable (P), and negatively ionizable (N)." During pharmacophore sites creation a default setting having H, D, A, P, N, and R was used and in the present study user-defined feature was not employed.

The pharmacophores were grouped together based on identical set of features with very similar spatial arrangements. A tree-based partitioning technique was used to identify common pharmacophores that groups similar pharmacophores as per their inter-site distances (ie, the site to site distances in the pharmacophore). After application of default feature definitions to each ligand, the common pharmacophores containing ≥ 5 sites using a terminal box size of 1° A were generated, where all of the active molecules should match. For alignment of the actives to the hypotheses and calculation of the score for the actives a score hypotheses step was employed. A hypothesis was provided by the developed pharmacophore which explained the binding of the active molecules to their receptors. This scoring procedure provides the positioning for the different hypotheses, and helps to make rational choices about the hypotheses which are mostly suitable for further investigations. Common pharmacophores with statistically significant values were chosen for molecular alignments.

3D-QSAR. PHASE module provides the basis of building the 3D-QSAR models by using the ligands activities that matches a reported hypothesis. "PHASE 3D-QSAR models are based on PLS regression, which applied to a large set of binary valued variables. In the QSAR model the independent variables are derived from a regular grid of cubic volume elements that span the space occupied by the training set ligands. Each ligand is represented by a set of bit values (0 or 1) that indicate which volume elements are occupied by a Van der Waals surface model of the ligand."

Table 2

Chemical structure of HPSA (compounds 34–80) employed for 3D-QSAR study along with predicted and actual pIC_{50} values against MMP-9 QSAR model II.

Compound (Ligand name)	R	R1	Actual pIC50	Predicted pIC50	Residual	Pharm Set	Fitness
34	OMe	Bn	5	4.78	−0.22	Moderate	3
35	OMe	3-Methoxy benzyl	5.05	4.78	−0.27	Moderate	2.95
36	OMe	3,4-Dichloro benzyl	5.22	4.88	−0.34	Active	2.97
37	OMe	4-Me benzyl	4.77	4.83	0.06	Active	2.98
38	OMe	2-Naphthylmethyl	5.3	4.92	−0.38	Active	2.9
39*	OMe	4-Biphenylmethyl	4.89	4.86	−0.03	Active	2.83
40*	OMe	Isoprenyl	4.41	4.44	0.03	Moderate	2.9
41*	OMe	4-Br benzyl	5	4.95	−0.05	Active	2.9
42	OMe	3-Ph propyl	4.89	4.14	−0.75	Inactive	2.58
43	OMe	*t*-Bu	3.19	4.15	0.96	Inactive	2.78
44	OMe	*n*-Bu	3.34	4.1	0.76	Inactive	2.74
45	OMe	Cyclo octyl	3.86	4.09	0.23	Inactive	2.76
46	OMe	Et	3.44	4.24	0.8	Inactive	2.77
47	OMe	Iso Pr	3.43	4.26	0.83	Inactive	2.75
48	OMe	Me	3.32	4.23	0.91	Inactive	2.79
49	O-n-Bu	Bn	5.4	5.56	0.16	Active	2.79
50	OMe	4-F benzyl	4.8	4.91	0.11	Active	2.9
51	O-n-Bu	4-F benzyl	4.72	4.9	0.18	Active	2.91
52*	OMe	4-Methoxy benzyl	4.92	4.89	−0.03	Active	2.96
53	OMe	4-Methoxy phenyl ethyl	4.47	4.14	−0.33	Inactive	2.69
54*	OMe	2-Ph ethyl	4.35	4.17	−0.18	Inactive	2.74
55	O-n-Bu	4-Methoxy benzyl	5.52	5.69	0.17	Active	2.75
56	OMe	3-Phenoxy propyl	4.36	4.14	−0.22	Inactive	2.58
57	O-n-Bu	3-Phenoxy propyl	5.3	4.72	−0.58	Active	1.66
60	OMe	4-[2-(1-Piperidinyl)ethoxy]benzyl	5.52	6.03	0.51	Active	2.53
61*	O-n-Bu	4-[2-(1-Piperidinyl)ethoxy]benzyl	5.7	5.81	0.11	Active	2.62
62*	O-n-Bu	3-[2-(4-Morpholinyl)ethoxy]benzyl	5.7	5.67	−0.03	Active	2.62
63	O-n-Bu	Me	5	4.47	−0.53	Moderate	2.67
64	O-n-Bu	Et	4.37	4.26	−0.11	Inactive	2.78
65	O-n-Bu	n-Bu	4.55	5.02	0.47	Active	2.7
66*	O-benzyl	Bn	5.52	5.56	0.04	Active	2.7
67	O-4Cl-Phenyl	Me	5.7	5.15	−0.55	Active	2.57
68	O-4Cl-Phenyl	Et	6	5.05	−0.95	Active	2.61
70	O-4Cl-Phenyl	Bn	6	6.23	0.23	Active	2.68
71	O-4Cl-Phenyl	H	5.7	4.84	−0.86	Active	1.9
72	O-Isopentyl	Bn	5.4	4.93	−0.47	Active	2.9
73	2-Ethylbutoxy	Bn	4.85	5.02	0.17	Active	2.81
74*	O-n-Bu	3-Methoxy benzyl	5.52	5.53	0.01	Active	2.75
75*	O-Me	4-(2-Thienyl)benzyl	4.96	4.89	−0.07	Active	2.87
76	O-Me	4-(2-Pyridinyl)benzyl	5.22	4.83	−0.39	Active	2.82
78	O-4Cl-Benzyl	4-Me benzyl	5.22	5.64	0.42	Active	2.68
79	2-Furanyl	Bn	5.52	5.12	−0.4	Active	2.47
80	O-4Cl-Phenyl	4-Methoxy benzyl	6	6.37	0.37	Active	2.66

3D-QSAR = 3-dimensional quantitative structure–activity relationship; MMP-9 = matrix metalloproteinase-9.
* Test compounds.

In order to distinguish between different types of atoms which occupy the same region of space, in the grid a given cube might be allocated as many as 6 bits, which accounts for 6 different atoms classes namely: hydrogen-bond donor (D), hydrophobic or non-polar (H), negative ionic (N), positive ionic (P), hydrogen-bond acceptors or electron-withdrawing (A) and other types (miscellaneous) (O).

PHASE generated 3D-QSAR models are either based on pharmacophore or on atoms, the only difference is either all atoms are considered, or only the pharmacophore sites which can be synchronized en route for the hypothesis. The selection of the type of model to develop mainly depends upon the fact that the training set molecules are congeneric and adequately rigid or not. The atom-based model can work well if the structures have some common structural framework and also contain a comparatively less number of rotatable bonds.[31]

Based on the criteria defined above, 2 atom-based 3D-QSAR models (QSAR models I and II) were generated for MMP-9 inhibitory activities by using the best 5 point AADDR (A-acceptor, D-donor, R-aromatic ring) and AAARP (A-acceptor, R-aromatic ring, P-positive ionic) hypothesis, respectively. The hypotheses were generated using 20 molecule training set for QSAR model I and 37 molecule training set for QSAR model II, and a grid spacing of 1.0 Q. 3D-QSAR models (I and II) with 1 to 3 PLS factors were generated and further, validated with predicting activities of molecules in the test set.

Results and discussion

Pharmacophore hypothesis generation

Ligand-based drug design is based on the understanding of known molecules which possesses biological activity to bind to

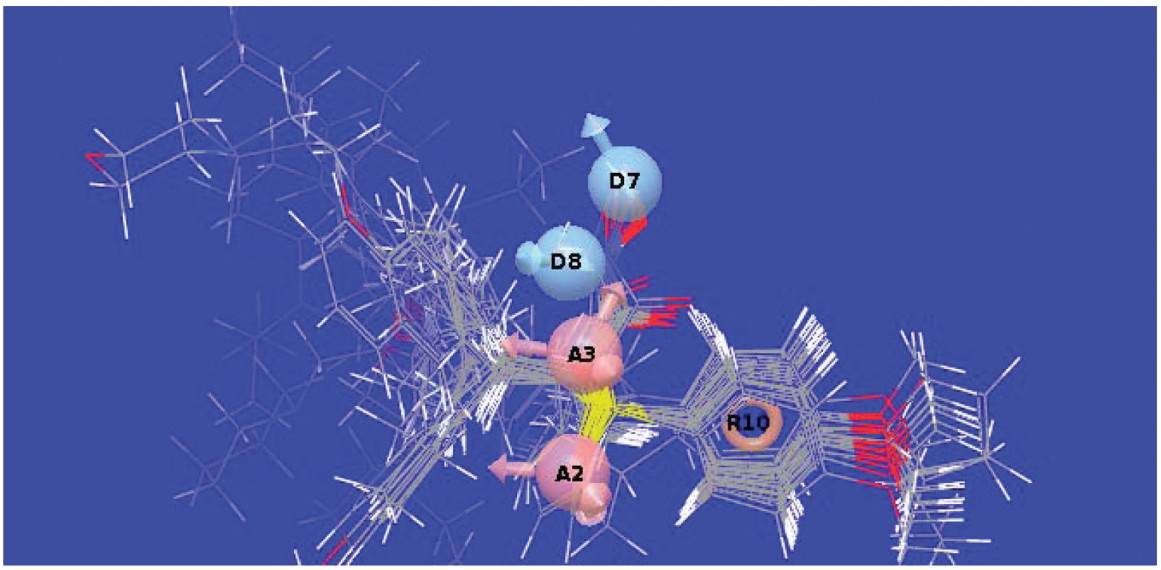

Figure 2. Pharmacophore model (AADDR) generated by PHASE for compounds 1 to 33. It illustrates hydrogen bond acceptors (A2, A3; pink color), (D7, D8; blue color), and aromatic ring (R10; orange color) features. All ligands overlapped on the generated model AADDR.

the target of concern. In order to bind to the target, a molecule must possess the minimum necessary structural characteristics and these molecules can be used to develop a pharmacophore.[32] The HPSAs derivatives tested as inhibitors for MMP by Aranapakam et al[18] were used in the current study to derive the pharmacophore models and to identify the necessary chemical features for the inhibitory effect. The structures of HPSAs employed in this work and their experimental values of the inhibitory activities were collected from the literature.[25] Previous reported studies discussed various linear and non-linear QSAR[24,25] approaches against MMP-1, MMP-9, and MMP-13, however, 3D-QSAR approach was not discussed.

Ligand based approaches consider two or three dimensional shape, chemistry, and pharmacophoric points to assess similarity. For identification of the common pharmacophore hypothesis, the experimental dataset was further divided into active and inactive sets. Molecules with pIC_{50} values $\geq$4.00 were considered to be active, and with pIC_{50} values $\leq$3.50 were considered as inactive, whereas those in-between were considered to be moderately active for QSAR model I. For QSAR model II, molecules with pIC_{50} values $\geq$4.80 were considered to be active, and with pIC_{50} values $\leq$4.40 were considered as inactive, whereas those in-between were considered to be moderately active. Selected pharmacophoric features for creating sites were A, H, R, N, and D. Pharmacophore models containing 3 to 6 features were generated for this study. The selection of best hypotheses was primarily dependent on best survival score which is a combination of active and inactive survival scores. For all the molecules in the dataset, the identification and creation of pharmacophoric sites was done followed by generation of common 5 point pharmacophore model with AADDR and AAARP hypothesis for MMP-9; QSAR model I and II, respectively. Further, these were subjected to stringent scoring function analysis. The common pharmacophore hypotheses were chosen based on a variant with a site score 0.91, vector score 0.991, and volume score 0.842. The best QSAR model I comprise of 2 hydrogen bond acceptors (A), 2 donors (D), and 1 aromatic ring (R) and was associated with the 5 point hypotheses. The hydrogen bond acceptors, donors, and aromatic ring were denoted as A1, A2, D1, D2, and R1. The best QSAR model II comprises of 3 hydrogen bond acceptors (A), 1 positive ionic (P), and 1 aromatic ring (R) and were associated with the 5 points hypotheses. The hydrogen bond acceptors, positive ionic, and aromatic ring were denoted as A1, A2, A3, R1, and P. Figures 2 and 3 represent the pharmacophore hypothesis (AADDR for QSAR model I and AAARP for QSAR model II) with all active molecules aligned to it. Further, the AADDR and AAARP hypothesis for QSAR models I and II, respectively, matched with all the molecules in the active set. For the generation of MMP-9 QSAR models I and II, the AADDR and AAARP pharmacophore hypothesis were used.

3D-QSAR studies (QSAR models I and II)

The 3D-QSAR studies for the HPSAs derivatives series were carried out using PHASE module of Schrodinger molecular modeling package to understand the effect of spatial arrangement of structural features on MMP inhibition. In the 3D-QSAR model generation, moderately active or inactive (non-modeled) molecules in the experimental dataset were aligned on the common pharmacophore hypothesis based on a match with at least 3 of the pharmacophoric features. For a QSAR study, the structural diversity in both the training and test set was given a bias, in order to form the standard 1:5 test set to training set ratio.

Tables 3 and 4 summarize the detailed statistics of the resulting 3D-QSAR models (I and II) based on random test set selection method. Selection of best PLS model is based on an employed statistical analysis which included the R^2 versus root-mean-square error (RMSE)/standard deviation (SD) plot. A minima is observed in the RMSE/SD value and a best model was chosen to be PLS factor model (PLS factor 3). For a reliable model, the squared predictive correlation coefficient should exceed 0.60.[33,34] In the selection of best model, criteria such as SD and RMSE were also taken into consideration. The statistically significant regression model was supported by the values of F (13.9 and 23.6 for QSAR models I and II, respectively), and small values of P (variance ratio), which is an indication of a high degree of confidence. Further, the small values of standard deviation of regression (0.31 and 0.33 for QSAR model I and II)

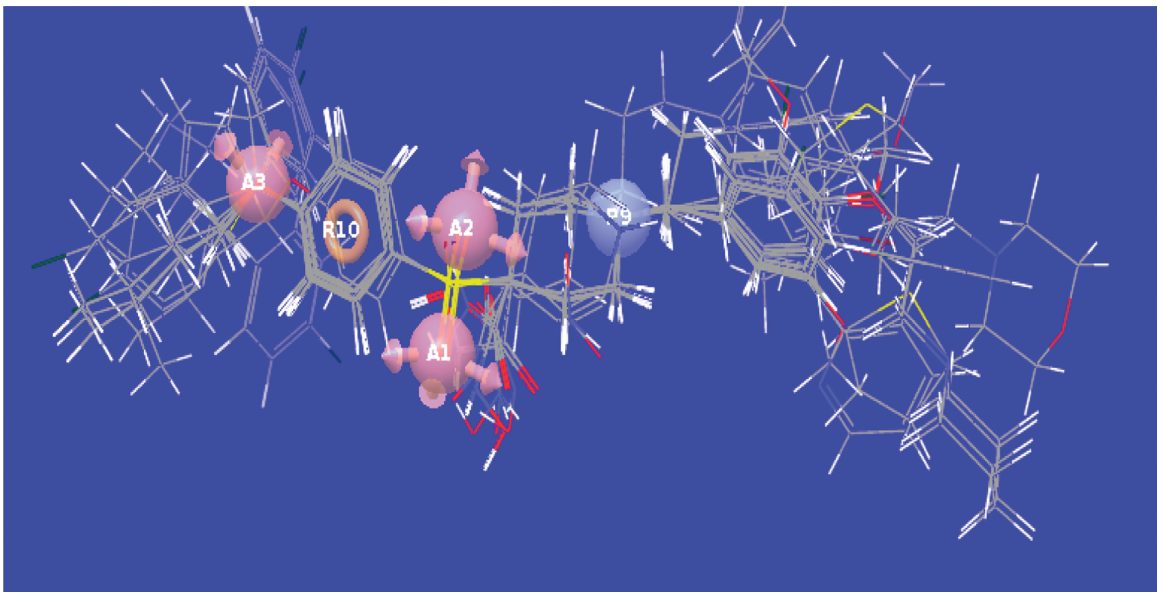

Figure 3. Pharmacophore model (AAARP) generated by PHASE for compounds 34 to 80. It illustrates hydrogen bond acceptors (A1, A2, A3; pink color), (P9; blue color), and aromatic ring (R10; orange color) features. All ligands overlapped on the generated model AAARP.

and RMSE (0.32 and 0.37 for QSAR models I and II, respectively) make an apparent inference that the data used for models generation are best for the QSAR analysis. It was further supported by the higher value of the QSAR model stability (0.61 and 0.83 for QSAR models I and II, respectively). A 3-PLS factor generated 3D-QSAR models with $R^2 = 0.61$ for QSAR model I and 0.63 for QSAR model II (random set selection), indicates a good correlation for the pharmacological activity. Figures 4(A and B) and 5(A and B) depict the linear plots of actual versus predicted activity for the training and test sets. The validity of each of the models was predicted from the calculated correlation coefficient for the randomly chosen test set comprising of diverse structures. The squared correlation for the test set (random selection $Q^2 = 0.84$ and 0.77 for QSAR models I and II, respectively) also signifies the good predictability of the final QSAR models for the test set. The Q^2 was more reliable and robust statistical parameter in comparison to R^2 as it is obtained by external validation method by randomly dividing the dataset into training and test set. Both the developed models (I and II) will be highly useful for predicting MMP-9 inhibitory activity of new compounds and could help in designing better molecules with enhanced anticancer activity.

Analysis of 3D-QSAR models (atom-based PHASE models)

The contribution of the substituents to the biological activity, whether positive or negative, could be predicted by the visualization of 3D characteristics of the all atom based QSAR model. Figures 6 and 7 depict 3D characteristics of the PHASE QSAR models and as the cubes represent the models and color codes as their coefficient values according to the sign. By default the blue color was for positive coefficients and red color was for negative coefficients. Further, an increase in biological activity was indicated by positive coefficients whereas a decrease in

Table 3

PHASE 3D-QSAR statistical parameters for compounds 1 to 33 (QSAR model I).

Statistical parameters (compounds 1–33)									
R^2	S.D.	*F* value	RMSE	R^2 cv	R^2 scramble	Q^2	Stability	Pearson *R*	*P*
0.61	0.31	13.9	0.32	0.65	−0.32	0.84	0.61	0.75	3.89e–05

Training set (N = 20) and test set (N = 7).

3D-QSAR = 3-dimensional quantitative structure–activity relationship, RMSE = root-mean-square error, SD = standard deviation.

Table 4

PHASE 3D-QSAR statistical parameters for compounds 34–80 (QSAR model II)

Statistical parameters (compounds 34–80)									
R^2	S.D.	*F* value	RMSE	R^2 cv	R^2 scramble	Q^2	Stability	Pearson *R*	*P*
0.63	0.33	23.6	0.57	0.64	−0.09	0.77	0.83	0.86	6.29e–07

Training set (N = 37) and test set (N = 10); *F* = the ratio of the model variance to the observed activity variance; *P* = significance level of *F* when treated as a ratio of Chi-squared distributions; Q^2 = directly analogous to R^2 but based on the test set predictions; R^2 = a coefficient of determination; RMSE = the RMS error in the test set predictions; SD = the standard deviation of regression; stability = stability of the model predictions to changes in the training set composition; Pearson *R* value for the correlation between the predicted activity and observed activity for the test set.

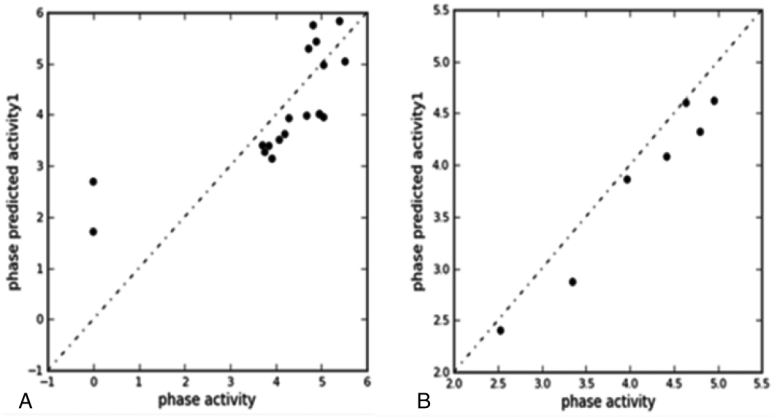

Figure 4. A and B: Graphical presentation of actual versus predicted pIC_{50} of training set and test set molecules for QSAR model I. QSAR = quantitative structure–activity relationship.

biological activity was indicated by the negative coefficients. In order to identify the characteristics of ligand structures whether to facilitate the increase or to decrease the activity the visualization of the coefficients was helpful. This might provide evidence to which functional groups were advantageous or non-advantageous at certain specific positions in a molecule. In 3D plots of the 3D pharmacophore regions the blue color cubes refer to ligand regions in which the specific attribute was important for enhanced biological activity, whereas the red cubes demonstrated that particular functional group or structural feature was not necessary for the biological activity or possibly the reason for decreased binding potency.

MMP-9 model (QSAR Model I). The volume occlusion maps shown in Figure 6 for MMP-9 atom based PHASE 3D-QSAR (QSAR model I) model (electronegative and hydrophobic) were represented by color codes. The occlusion maps symbolize the regions of favorable and unfavorable interactions.

The volume occlusion maps of electron-withdrawing groups shown in Figure 6A indicated the suitable position of electron-withdrawing groups attached on the C1 position of the phenyl ring of the HPSAs moiety. The presence of large number of blue cubes due to the presence of number of electron withdrawing moieties such as oxygen, nitrogen, etc. further supported the increase in activity. The analysis was suggestive that the improvements in the MMP-9 inhibitor binding affinity can be achieved by substituting electron-withdrawing groups on the phenyl ring of HPSAs moiety at C1 positions. Also, the positive potential of electron withdrawing attributes of the molecules and was essential for the MMP-9 activity at this particular position.

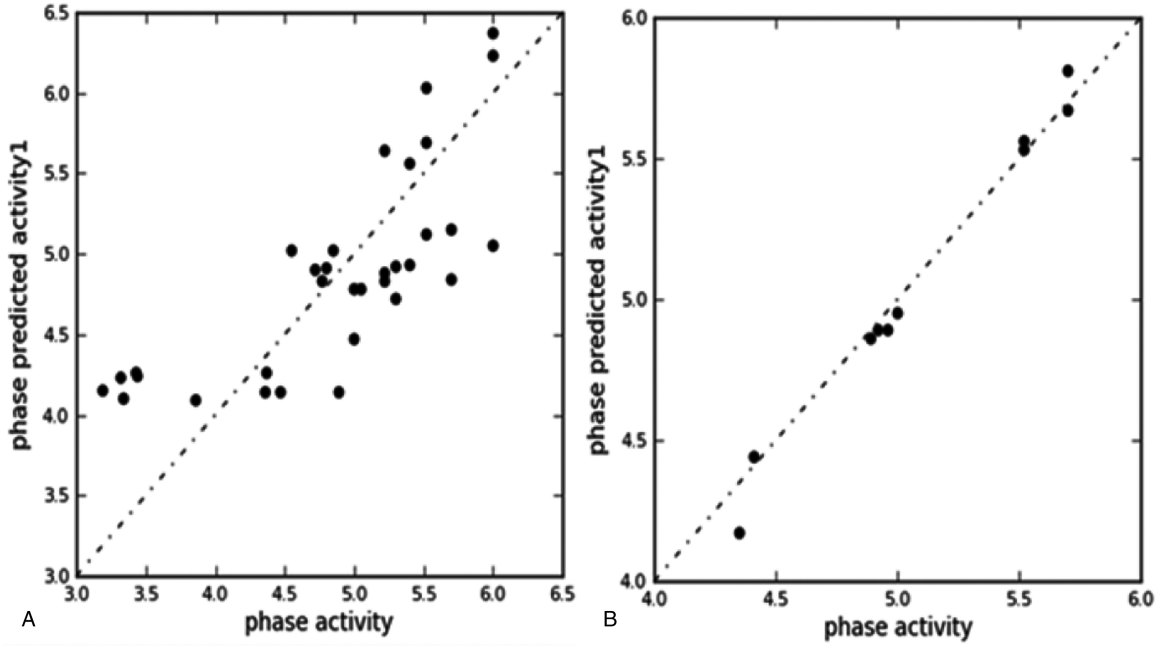

Figure 5. A and B: Graphical presentation of actual versus predicted pIC_{50} of training set and test set molecules for QSAR model II. QSAR = quantitative structure–activity relationship.

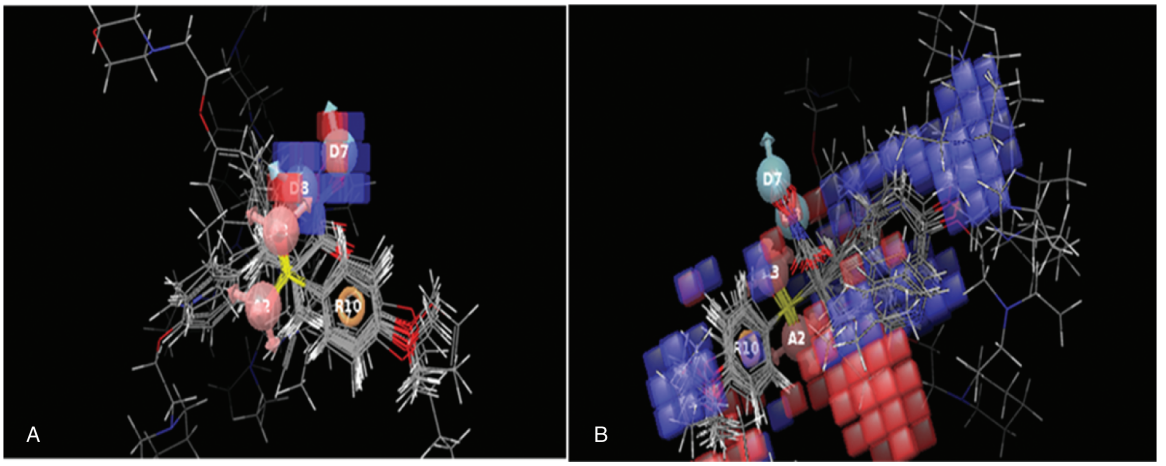

Figure 6. (A and B): Visual representation of atom-based PHASE 3D-QSAR (MMP-9 QSAR model I). A: Hydrogen bond donor; electron withdrawing, and B: hydrophobic. Blue color cubes indicate positive coefficient or increase in activity and red color cubes indicate negative coefficient or decrease in activity. QSAR = quantitative structure–activity relationship.

However, other positions were not favorable for the electron withdrawing groups and probably will contribute to decrease in the MMP-9 activity.

Hydrophobic volume occlusion maps (Fig. 6B) showed blue colored cubes on C1 and C5 positions of phenyl ring demonstrating that an increase in the hydrophobic character in this region probably improved the activity of the HPSAs type molecules. Also, at the C2 (ortho) position the rich density of blue colored cubes was further suggestive of increase in activity. The red colored cubes on C3 positions were not favoring the assignment of hydrophobic groups.

Based upon analysis, the all atom QSAR model I generated by PHASE depicts that substitution at C1 position of phenyl ring played a vital role in the MMP-9 inhibitory activity. The substitutions at other positions, that is, C3 and C6 were not having any significant contribution in the biological activity.

MMP-9 model (QSAR Model II). The volume occlusion maps shown in Figure 7 for MMP-9 atom based PHASE 3D-QSAR (QSAR model II) model (hydrogen bond acceptor, hydrophobic) were represented by color codes. The occlusion maps symbolize the regions of favorable and unfavorable interactions.

Visually, Figure 7A analysis illustrated the presence of the blue color cubes near and around the hydrogen acceptor site (A1) which positively contributed to MMP-9 inhibition. Further, the presence of blue cubes at C2 position of the phenyl ring was also suggestive of increase in activity. Also the presence of blue cubes near to positive ionic feature described the favorable ionic interactions. The availability of red color cubes at C1 position of phenyl rings resulted in decreased activity.

Figure 7B illustrates the effect of hydrophobic groups on MMP-9 inhibitory activity. Inference can be drawn from the picture that hydrophobic groups (blue cubes) were well tolerated near C1, C4, and C6 positions of the phenyl ring on HPSAs moeity, whereas the substitution of hydrophobic groups at C2, C3, C5 of the phenyl ring site were intolerable (red cubes) or may hamper the binding of the molecules to the active site receptor which resulted in decreased MMP-9 inhibition.

Based on above analysis, the all atom QSAR model II generated by PHASE depicted that substitution at C1 and C4 by different

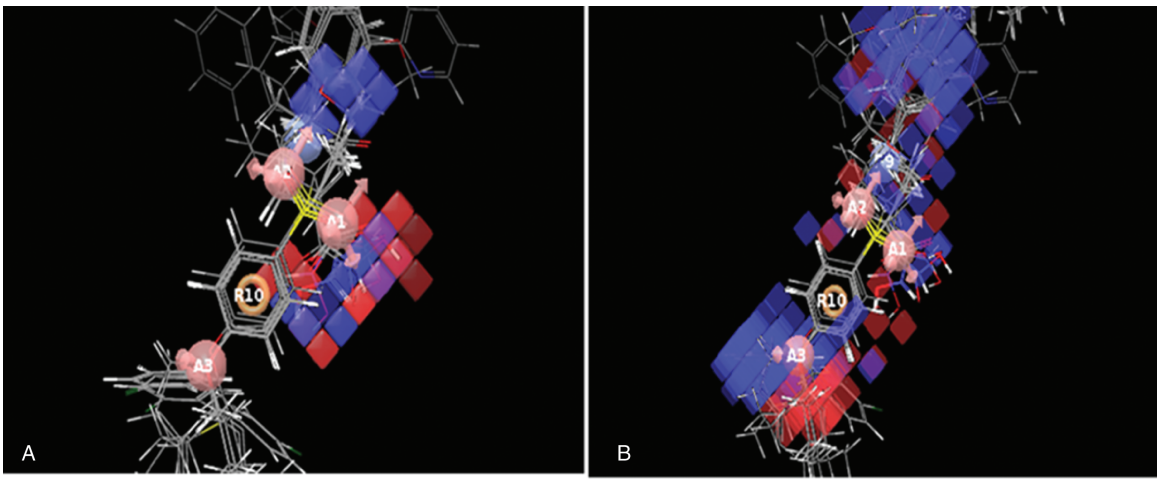

Figure 7. (A and B): Visual representation of atom-based PHASE 3D-QSAR model (MMP-9 QSAR model II). A: Hydrogen bond acceptor; and B: hydrophobic. Blue color cubes indicate positive coefficient or increase in activity and red color cubes indicate negative coefficient or decrease in activity.

groups like hydrogen acceptor, positive ionic, and/or hydrophobic groups play an important role in the MMP-9 activity. The substitutions at other positions, that is, C2, C3, and C5 were not having any significant contribution in the biological activity.

Conclusion

The two atom-based pharmacophoric 3D-QSAR models (I and II) were successfully developed for a set of MMP-9 inhibitory activity of HPSAs derivatives. The obtained models exhibit good fitness with the experimental data, with a maximum correlation coefficient of 0.61 for QSAR model I and 0.63 for QSAR model II and having hydrophobic and H-bond acceptor and H-bond donor features as crucial parameters for MMP-9 inhibition. Furthermore, cross-validation coefficient ($Q^2 = 0.84$ and 0.77 for QSAR models I and II, respectively) reflected good predictive power of the models. Robustness of the models was indicated by the higher degree of closeness between experimental and predicted activity. Therefore, the developed 3D-QSAR models (I and II) could be employed to predict MMP-9 inhibitory activity of HPSAs derivatives. This will further add in designing better molecules with enhanced MMP-9 inhibitory activity.

Acknowledgments

The authors wish to thank Department of Pharmaceutical Sciences, M.D. University, Rohtak and the management of JCDM college of Pharmacy for providing the facilities and uninterrupted support to carry out the work. This research did not receive any specific grant from funding agencies in the public, commercial, or not-for-profit sectors.

Authors' contributions

VL recommended the topic, designed the procedures and experiments for the work and supervised the entire study. HD was involved in the instigation of the proposal, reviewed the manuscript decisively, and has provided final version approval to be published. DR performed the in silico studies, completed data analysis, and interpretation of results and arranged the draft of the manuscript. VL improved the manuscript. All the authors read and approved the final manuscript.

Conflicts of interests

Authors declare that they have no competing interests. The authors alone are responsible for the content and writing of the research paper.

References

[1] Bauvois B. New facets of matrix metalloproteinases MMP-2 and MMP-9 as cell surface transducers: outside-in signaling and relationship to tumor progression. Biochim Biophys Acta. 2012;1825:29–36.
[2] Kessenbrock K, Plaks V, Werb Z. Matrix metalloproteinases: regulators of the tumor microenvironment. Cell. 2010;141:52–67.
[3] Page-McCaw A, Ewald AJ, Werb Z. Matrix metalloproteinases and the regulation of tissue remodelling. Nat Rev Mol Cell Biol. 2007; 8:221–233.
[4] Parks WC, Wilson CL, López-Boado YS. Matrix metalloproteinases as modulators of inflammation and innate immunity. Nat Rev Immunol. 2004;4:617–629.
[5] Visse R, Nagase H. Matrix metalloproteinases and tissue inhibitors of metalloproteinases: structure, function, and biochemistry. Circ Res. 2003;92:827–839.
[6] Westermarck J, Kähäri VMJ. Regulation of matrix metalloproteinase expression in tumor invasion. FASEB J. 1999;13:781–792.
[7] Gialeli C, Theocharis AD, Karamanos NK. Roles of matrix metalloproteinases in cancer progression and their pharmacological targeting. FEBS J. 2011;278:16–27.
[8] Sarvaiya PJ, Guo D, Ulasov I, et al. Chemokines in tumor progression and metastasis. Oncotarget. 2013;4:2171–2185.
[9] Campbell NE, Kellenberger L, Greenaway J, et al. Extracellular matrix proteins and tumor angiogenesis. J Oncol. 2010;2010:586905.
[10] Solovyeva NI, Vinokurova SV, Ryzhakova OS, et al. Expression of gelatinases A and B and their endogenous regulators in immortal and transformed fibroblasts. Biomed Khim. 2009;55:441–450.
[11] Ye HQ, Azar DT. Expression of gelatinases A and B, and TIMPs 1 and 2 during corneal wound healing. Invest Ophthal Visual Sci. 1998;39:913–921.
[12] Forsyth PA, Laing TD, Gibson AW, et al. High levels of gelatinase-B and active gelatinase-A in metastatic glioblastoma. J Neurooncol. 1998;36:21–29.
[13] Vandooren J, Van den Steen PE, Opdenakker G. Biochemistry and molecular biology of gelatinase B or matrix metalloproteinase-9 (MMP-9): the next decade. Critical Rev Biochem Mol Biol. 2013;48:222–272.
[14] Purcell WT, Rudek MA, Hidalgo M. Development of matrix metalloproteinase inhibitors in cancer therapy. Hematol Oncol Clin North Am. 2002;16:1189–1227.
[15] Rowsell S, Hawtin P, Minshull CA, et al. Crystal structure of human MMP9 in complex with a reverse hydroxamate inhibitor. J Mol Biol. 2002;319:173–181.
[16] Tandon A, Sinha S. Structural insights into the binding of MMP-9 inhibitors. Bioinformation. 2011;5:310–314.
[17] Kalva S, Vadivelan S, Sanam R, et al. Lead identification and optimization of novel collagenase inhibitors; pharmacophore and structure based studies. Bioinformation. 2012;8:301–308.
[18] Aranapakam V, Grosu GT, Davis JM, et al. Synthesis and structure–activity relationship of α-sulfonylhydroxamic acids as novel, orally active matrix metalloproteinase inhibitors for the treatment of osteoarthritis. J Med Chem. 2003;46:2361–2375.
[19] Almstead NG, Bradley RS, Pikul S, et al. Design, synthesis, and biological evaluation of potent thiazine- and thiazepine-based matrix metalloproteinase inhibitors. J Med Chem. 1999;42:4547–4562.
[20] Donini OAT, Kollman PA. Calculation and prediction of binding free energies for the matrix metalloproteinases. J Med Chem. 2000;43:4180–4188.
[21] Pirard B, Matter H. Matrix metalloproteinase target family landscape: a chemometrical approach to ligand selectivity based on protein binding site analysis. J Med Chem. 2006;49:51–69.
[22] Gupta SP, Kumaran S. A quantitative structure–activity relationship study on clostridium histolyticum collagenase inhibitors: roles of electrotopological state indices. Bioorg Med Chem. 2003;11:3065–3071.
[23] Kalva S, Vinod D, Saleena LM. Field and Gaussian-based 3D-QSAR studies on barbiturate analogs as MMP-9 inhibitors. Med Chem Res. 2013;22:5303–5313.
[24] Du H, Wang J, Watzl J, et al. Prediction of inhibition of matrix metalloproteinase inhibitors based on the combination of Projection Pursuit Regression and Grid Search method. Chem Intell Lab Syst. 2008;93:160–166.
[25] Fernandea M, Caballero J. QSAR modeling of matrix metalloproteinase inhibition by N-hydroxy-α-phenylsulfonylacetamide derivatives. Bioorg Med Chem. 2007;15:6298–6310.
[26] Phase, Version 3.0. Schrodinger LLC, New York, NY; 2008.
[27] Maestro, Version 8.5. Schrödinger, LLC, New York, NY, USA; 2008.
[28] Lather V, Kristam R, Singh JS, et al. QSAR models for prediction of glycogen synthase kinase-3β inhibitory activity of indirubin derivatives. QSAR Comb Sci. 2008;27:718–728.
[29] Kaminski A, Friesner RA, Tirado-Rives J, et al. Evaluation and reparametrization of the opls-aa force field for proteins via comparison with accurate quantum chemical calculations on peptides. J Phy Chem B. 2001;105:6474–6487.
[30] Amnerkar ND, Bhusari KP. Synthesis, anticonvulsant activity and 3D-QSAR study of some prop-2-eneamido and 1-acetyl-pyrazolin derivatives of aminobenzothiazole. Eur J Med Chem. 2010;45:149–159.
[31] Katritzky AR, Mu L, Lobanov VS, et al. Correlation of boiling points with molecular structure. 1. A training set of 298 diverse organics and a test set of 9 simple inorganics. J Phys Chem. 1996;100:10400–10407.
[32] Guner OF. Pharmacophore perception, development, and use in drug design. IUL Biotechnology Series. International University Line, San Diego, Calif, USA:2000.
[33] Dureja H, Kumar V, Gupta S, et al. Topochemical models for the prediction of lipophilicity of 1,3-disubstituted propan-2 one analogs. J Theor Comp Chem. 2007;6:435–448.
[34] Wold S. Validation of QSAR's. Quant Struct Act Relat. 1991;10:191–193.